

Gravity-driven, dry granular flows over a loose bed in stationary and homogeneous conditions

Sabrina Meninno,^{*} Aronne Armanini,[†] and Michele Larcher[‡]

DICAM-CUDAM, University of Trento, Trento, Italy



(Received 26 May 2017; published 5 February 2018)

Flows involving solid particulates have been widely studied in recent years, but their dynamics are still a complex issue to model because they strongly depend on the interaction with the boundary conditions. We report on laboratory investigations regarding homogeneous and steady flows of identical particles over a loose bed in a rectangular channel. Accurate measurements were carried out through imaging techniques to estimate profiles of the mean velocity, solid concentration, and granular temperature for a large set of flow rates and widths. Vertical and transversal structures observed in the flow change as interparticle interactions become more collisional, and they depend on the bottom over which the flow develops. The lateral confinement has a remarkable effect on the flow, especially for narrow channels compared with the grain size, and a hydraulic analogy is able to show how the walls influence the mechanisms of friction and energy dissipation.

DOI: [10.1103/PhysRevFluids.3.024301](https://doi.org/10.1103/PhysRevFluids.3.024301)

I. INTRODUCTION

Dry granular flows driven by gravity are an important paradigm for a large number of problems, from industrial applications to geophysical processes. Flows of this type are strongly influenced by the boundary conditions imposed at the bottom, as proven by the variety of the behaviours described in the literature. Most of the published investigations regard inclined granular flows over a bumpy and flat rigid base, while only a few of them focus on fully developed, steady flows over an erodible bed. This kind of flow is important to understand the dynamics of complex phenomena such as dense snow avalanches and some types of landslides, which usually move on a loose deposit made of the same material that composes the flow. In such situation, the erodible bed forms spontaneously and is dynamically coupled with the material flowing over it.

Looking at steady free-surface flows, which occur above a threshold value of the surface inclination [1,2], experimental observations have pointed out the dependence of the slope on the discharge [3,4] and on the lateral confinement [5–7], which allows the flow to reach angles steeper than the friction angle of the material.

Unlike flows over a rigid bottom that display "Bagnold-type" velocity profiles [8,9], in the case of dense flows over a loose bed, the velocity profile is characterized by an exponential tail towards the granular bed, where Komatsu *et al.* [10] observed a slow creeping. Except near the free surface, concentration is often assumed constant along the flow depth, with values close to the loose packing concentration [11]. However, an analysis on how profiles of the concentration and the granular temperature evolve with increasing flow rates is still missing.

^{*}Present address: CERIS, Instituto Superior Técnico, Universidade de Lisboa, Lisbon, Portugal; meninno.sabrina@gmail.com

[†]aronne.armanini@unitn.it

[‡]Present address: Faculty of Science and Technology, Free University of Bozen-Bolzano, 39100 Bozen-Bolzano, Italy; michele.larcher@unibz.it

When treating granular materials, another open question is the role of the boundary conditions on the flow behavior, such as the slip velocity and the shear rate at the bed [12]. In flows over a rigid base, for example, bottom roughness controls both the depth of the stopping flow, h_{stop} [13], and the slip velocity [14]. Additionally, simulations by Kumaran *et al.* [15] and Silbert *et al.* [16] prove that the system passes from a disordered state to an organized state with changing values of the relative roughness of the bottom, d/d_w . On the contrary, smooth bottom surfaces seem to cause only local variations in the flow properties, and they affect the slip at the solid interphase where shear is more intense. Focusing on confined flows, Artoni *et al.* [17] report some numerical results showing a correlation between the effective friction $m_w = \tau/p$ and the velocity at sidewalls, using the velocity fluctuations at the walls as the scale of the problem. The same scaling emerges in the theoretical analysis developed in the framework of kinetic theory [18] for fully collisional systems [19,20], where the ratio between the tangential and the normal forces at the sidewalls is considered proportional to the ratio between the mean velocity and the granular temperature at the same location, through different factors depending on the types of collisions experienced by the grains (sticking or sliding).

All these aspects add complexity to the theoretical description of granular flows, whose rheology still poses a challenge for researchers. Two limit regimes are commonly recognized in free-surface flows [21,22]: one is characterized by low concentration and binary and quasi-instantaneous collisions among particles (collisional regime or granular gas phase), and the other one (frictional regime) is dominated by long-lasting contacts between grains. In the intermediate region, or liquid phase, short- and long-term interactions coexist and are intermittent [23], and temporary force networks can develop. Obtaining precise measurements of what happens inside the flow is of primary importance in order to develop a rheology based on physical observations and to test the models against real data.

The issues specifically addressed in this paper are the following:

(1) the measurements of the vertical and crosswise patterns of the streamwise velocity, granular temperature, and concentration for a range of flow conditions that span from very slow flows to very fast ones; and

(2) the assessment of the effects of the boundaries on the investigated variables, especially by varying the channel width and the bottom conditions.

Section II is devoted to the description of the experimental setup and the techniques used to collect data. The principle of the used imaging technique is briefly explained. In Sec. III, the results are shown, presenting the profiles of velocity, concentration, and granular temperature for different ranges of investigation. In Sec. IV, the results are discussed and interpreted, while Sec. V draws the conclusion of the work.

II. METHODS

The experimental setup was designed to reproduce free-surface flows of dry granular materials over a loose deposit. Measurements of the flow field were achieved through automated imaging techniques to obtain profiles of velocity, concentration, and granular temperature both from the sidewalls and along the free surface.

A. Experimental facility and types of investigation

The granular material used in the tests was made up of plastic particles having a spherical shape and an opaque color. The beads have a mean diameter of 0.55 ± 0.05 mm and a material density of 980 ± 2.7 kg m⁻³, while the mean frictional angle was estimated to be $24.5 \pm 0.5^\circ$ through the funnel test, by measuring the steepest slope at which the grains could be piled.

The experimental facility consists of an open channel having transparent sidewalls made of perspex, a hopper to convey the material into the flume, and a tank to collect the grains at the outlet of the chute. The system is an open circuit, in which the flow rate is controlled by the opening of the hopper, and it is verified by weighting the material collected at the end of the flume in a given lapse of time when the flow is steady.

The channel is 2.5 m long and 15 cm wide, but can be narrowed by placing a partition wall. The bottom is artificially roughened by coarse sandpaper, and its slope angle can be changed from 0 to 45° thanks to a hydraulic piston that is mounted upstream. The outlet section of the flume is closed by a multiple slit gate, used to control the flow and to induce the formation of a static deposit inside the channel. This deposit is stabilized by the material flowing over it and it extinguishes as the flow stops.

The experimental setting is equipped with two synchronized high-speed cameras (Photron Fastcam 1024PCI) to record and analyze the flow field. Image acquisition at different frame rates was needed to resolve particle velocities over different orders of magnitude. The highest acquisition frequency adopted in the recordings was $f_{ac} = 3000$ fps for high flow rates, while at low discharges the frequency was limited at $f_{ac} = 500$ fps, allowing for longer duration and larger image sizes. The resolution was chosen each time to have the best field of view necessary to compute the velocity profiles in the vertical or in the transversal direction. The cameras were oriented downwards, normal to the channel bottom, to analyze the surface flow field, or pointing the flow through the perspex sidewalls, to analyze the vertical structures of the flow. In the latter case, the cameras were tilted to align the observation window with the inclined flume.

B. Imaging techniques

Imaging techniques were used to evaluate the velocity field both from the top surface of the flow and from the lateral sidewalls. Homemade algorithms, developed within a collaboration between the University of Trento, the Université Catholique de Louvain, and the National Taiwan University, were used to analyze the recordings, employing the Voronoï technique developed and fully described in [24,25].

This method can be included in the class of the particle-tracking algorithms, and it exploits the Voronoï tessellation of the space to track particles in subsequent frames of a recording.

Briefly, the algorithms used to process the images perform the following operations:

(1) identifying the particle centers in the entire sequence of images with a subpixel accuracy. Particles are initially highlighted by applying a Laplacian-of-Gaussian filter to images, and then their position are identified by pinpointing the local brightness maxima.

(2) matching particles in subsequent frames to track them in time. This step is performed by recognizing the similarity between the Voronoï diagrams built on the particle centers of successive frames.

The method is able to track identical particles even for high density and different shear rate across the frame. In fact, the polygons divide the space into nonoverlapping parts with their own centroids, which remain almost unchanged for small time intervals, allowing the identification of the same patterns in subsequent images. After pairing each particle frame to frame, the velocity vectors are defined as

$$\mathbf{v}_i^n = \frac{\mathbf{r}_i^{(n+1)} - \mathbf{r}_i^{(n)}}{\Delta t}, \quad (1)$$

where $\mathbf{r}_i^{(n)} = (x_i^{(n)}, y_i^{(n)})$ is the two-dimensional position of the i th particle at time $t^{(n)}$, and $\mathbf{v}_i^{(n)} = (u_i^{(n)}, v_i^{(n)})$ is the corresponding in-plane velocity in the x and y axes oriented in the directions parallel and orthogonal to the flow direction. By using two synchronized cameras to record the flow, the out-of-plane velocity component $w_i^{(n)}$ can be computed, along the z axis normal to the sidewalls. A calibrated scale factor allows the transformation from pixel to physical coordinates.

The instantaneous velocity fluctuations are used to compute the granular temperature, which represents a measure of the kinetic energy owned by the particles. It is defined as

$$T = \frac{1}{3} (\langle u_i^2 \rangle + \langle v_i^2 \rangle + \langle w_i^2 \rangle), \quad (2)$$

where T is the granular temperature. The brackets $\langle \cdot \rangle$ designate a spacial average performed on flow-oriented layers, while $u'_i = u_i - \langle u \rangle$, $v'_i = v_i - \langle v \rangle$, and $w_i = w_i - \langle w \rangle$ are the velocity fluctuations

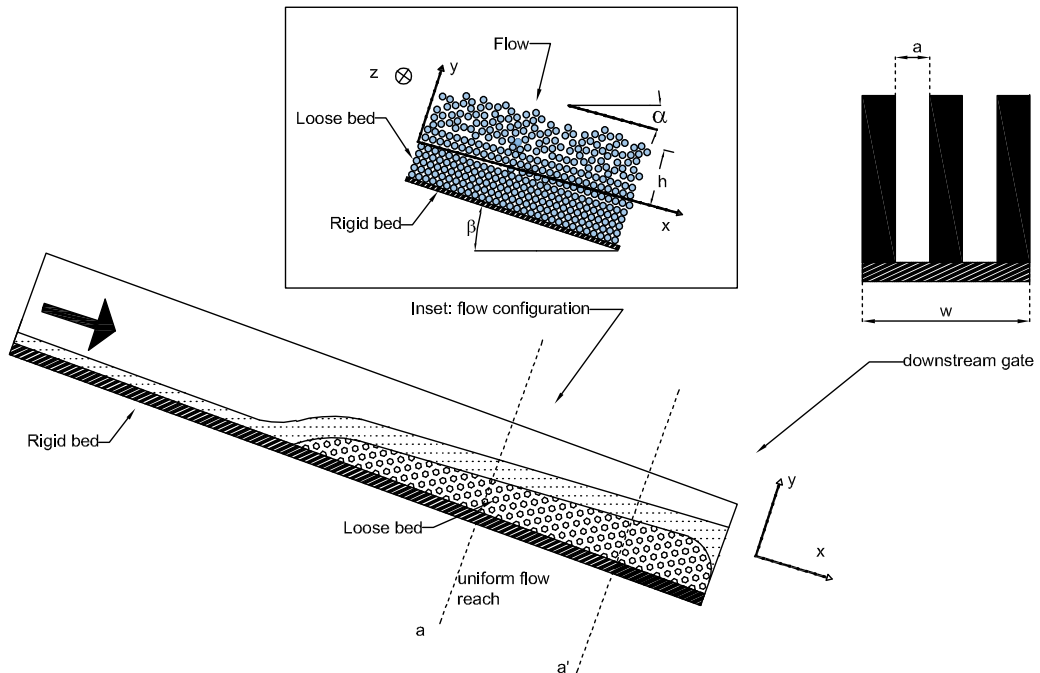


FIG. 1. Sketch of the flow: the rigid bed corresponds to the channel base, while the loose bed corresponds to the interphase between moving grains and particles at rest. The xyz system is based on the flow direction. β is the tilting angle of the flume, while α is the slope of the free surface.

of the grains along the direction parallel and normal to the bed, and along the direction normal to the sidewall.

The Voronoï diagrams are also exploited to compute the near-wall volumetric concentration, as shown by Capart *et al.* [24] and Spinewine *et al.* [25].

III. MEASUREMENTS

The experiments refer to fully developed flows in a rectangular channel and over a loose bed. The flow is three dimensional and the presence of a static deposit is induced by the presence of a gate with multiple openings at the end of the flume (see Fig. 1). For all the runs, the flume is inclined with a slope greater than the internal friction angle of the material, in order to obtain a part where the material flows on a rigid rough base, and another part where a mobile bed is developed, as clarified in Sec. III D. In the latter region, the deposit height and the extension of the uniform flow are controlled by the downstream gate varying the width of its apertures, and the free surface is parallel to the deposit where the flow is uniform. The experimental evidences displayed in Fig. 2 show that the mobile bed slope depends only on the volumetric discharge, as observed also in sediment transport in rivers, remaining unchanged by varying the slit aperture of the gate. Thus, under statistically homogeneous and stationary conditions (statistically uniform flow) and for the same flume geometry, the flow conditions can be related solely to the flow rate, as long as the height of the deposit remains high enough to act as an absorber by preventing the rigid bed from reflecting back the energy of the upper flows. According to our observations, compared to a simple weir, the gate guarantees longer portions of uniform flows since it minimizes the disturbance effects at the outlet of the flume.

As represented in Fig. 1, the flow depth h is measured from the static deposit to the free surface y_{surf} , while W is the width of the flume. In addition, the identification of the loose bed is facilitated by observing that the slope of the deposit is equal to the free-surface slope in uniform flow conditions.

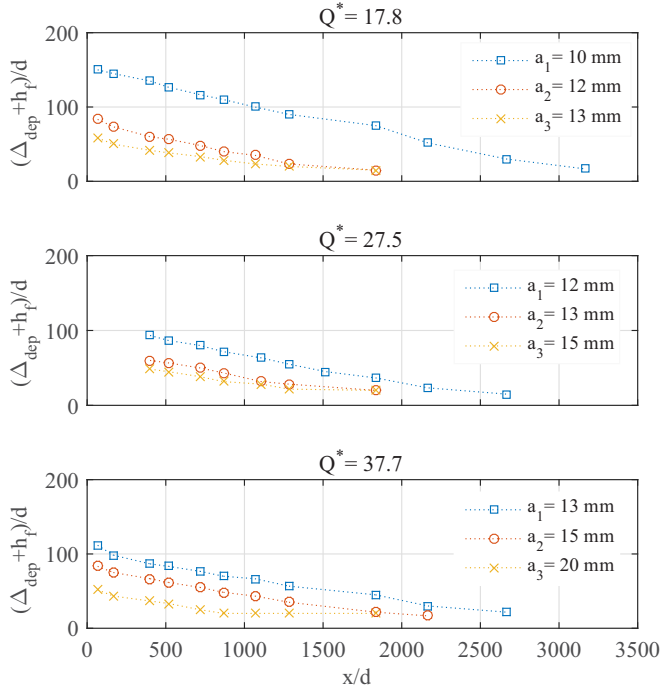


FIG. 2. Behavior of the deposit Δ_{dep} and the flow depth h_f measured from the fixed bed, for different flow rates and different apertures of the slit gate ($a_1 < a_2 < a_3$). The deposit keeps the same slope changing the aperture of the gate for the same flow rate.

The measurements were made in correspondence to the sections where the flow reaches the uniform conditions, far from the outlet and inlet of the channel. In these regions, it was accurately verified that the flow field remained unperturbed and steady in time and homogeneous in the x direction.

A. Scales

The results are presented by considering the average values of each variable in time. For each frame, the analysis window that includes the whole flow depth is divided into nonoverlapping stripes, whose height is usually equal to 1.5 particle diameter. The mean velocity, the granular temperature, and the concentration are computed in each layer, first by performing a spatial average over the particles whose centroids fall in the layer itself and then by averaging over time these instantaneous values. The nondimensional flow rate Q^* is computed by normalizing the volumetric discharge with $dW\sqrt{gd}$, which corresponds to the grain scale, in order to compare the results to some of the literature data. Velocity and granular temperature are expressed using the international system of units.

B. Near-wall profiles of velocity, concentration, and granular temperature

Overall, particle dynamics can be inferred first from grain trajectories in the xy plane. While near the free surface particles fluctuate clearly even in the vertical direction, towards the bed they tend to move mainly in the longitudinal direction. However, momentum is constantly transmitted from one layer to another thanks to the repeating chattering of the particles, but if Q^* is sufficiently large, the velocity fluctuations are strong enough to push a particle to jump between strata. Once this occurs, a void is left and a new particle is free to move into the new available space. Armanini *et al.* [23] found the same evidence for mixtures of solids and water, and Hill *et al.* [26] observed the same behavior in

their rotating drum experiments. They pointed out that there is always a strong component of order, which results in a stratification parallel to the mean flow, superposed with a intermittent component of disorder (self-diffusion perpendicular to the mean flow). For layers near the static deposit, the motion tends to correspond to a slow rearrangement of particle positions, and the vertical movements are strongly controlled by the formation of the voids, which become more rare. The free surface is characterized by a higher agitation with respect to the strata below. Particles continuously jump one over each other, mixing together and traveling longer paths with respect to the lower layers, although in our case their ballistic trajectories are flat, as shown in Fig. 4 for the case of a single frame.

Figure 3 reports a sample of the normal-to-bed profiles measured in different runs and distinguished into three groups according to their discharge.

The classification of the experiments according to the three ranges of the flow rates is related to the relative size of the regions characterized by the collisional activity within the flow. Passing from very slow flow rates to high flow rates, collisions start to play a progressively more important role in the global behavior of the flow. Looking at the experiments and considering how the variables change, three categories can be distinguished: (i) $Q^* = [0-10]$, where the collisional part is practically absent; (ii) $Q^* = [40-90]$, which is an intermediate stage between the other classes; and (iii) $Q^* > 90$, where collisions are relevant in the overall behavior of the flow (see Ref. [27] for the complete set of the measurements). It is useful to specify that this classification cannot be taken literally, but it must be understood more qualitatively than quantitatively.

Velocity, concentration, and granular temperature are measured through an optical method that tracks all the observed particles in a control volume with an extension that might change according to the frame rate, but it is usually equal to 20×20 mm, as shown in Fig. 4. Each point in the vertical profile is a temporal and spatial average of all the detected particles falling in each layer. Thus, the values of velocity, concentration, and granular temperature reported in the paper must be understood as averaged values in the control volume and in a sufficiently long temporal interval. The vertical position of the free surface is defined as the center of the layer at which the concentration is very low and falls to a value of 0.01. This layer might include salting particles and ballistic trajectories.

As expected, velocity and granular temperature are all continuously varying throughout the flow depth from the top free surface down to the bed, but also the concentration appears nonconstant.

Generally, the longitudinal velocity appears to decay as the distance from the surface increases, vanishing towards the loose bed with an exponential tail. However different behaviors emerge at increasing discharges, as the collisional regime starts dominating in the flow: (i) for very low discharges Q^* , the velocity distribution remains concave as it reaches the top layers; (ii) for high discharges Q^* , the velocity profile shows a kink above the half of the flow depth followed by a reverse concavity, which seems to suggest the presence of a region where the flow is more diluted; and (iii) in the intermediate cases, the velocity increases sharply towards the top layers, where the more agitated particles collide against each other and are free to move.

The transition from a configuration dominated by friction to a configuration controlled by collisions is also highlighted by the trend observed in the concentration profiles. Generally speaking, the concentration remains almost comparable to the random loose packing value for a large part of the flow depth, and then it progressively decreases towards the surface, starting from almost half the depth. However, higher discharges are characterized by a strong gradient throughout the depth, while in the other cases the variation is confined near the free surface.

In accordance with the overall behavior, the granular temperature increases going to the top, and it gradually diminishes near the bottom where particles are trapped in their static configuration.

In Fig. 3, three different regions are highlighted along the vertical profiles, based on observations of the shape and values of velocity and concentration profiles as follows: (i) flow dominated by collisions (d.c.), where the concentration is very low (<0.4), and the velocity profiles show a change in slope; (ii) intermediate region, which is a “transitional” region; (iii) flow dominated by friction (d.f.), where the particle concentration is practically equal to the random loose packing concentration, while the velocity profile is concave with an exponential tail towards the loose bed; and (iv) loose bed, which starts from the level where the material is not moving. We determined this elevation by

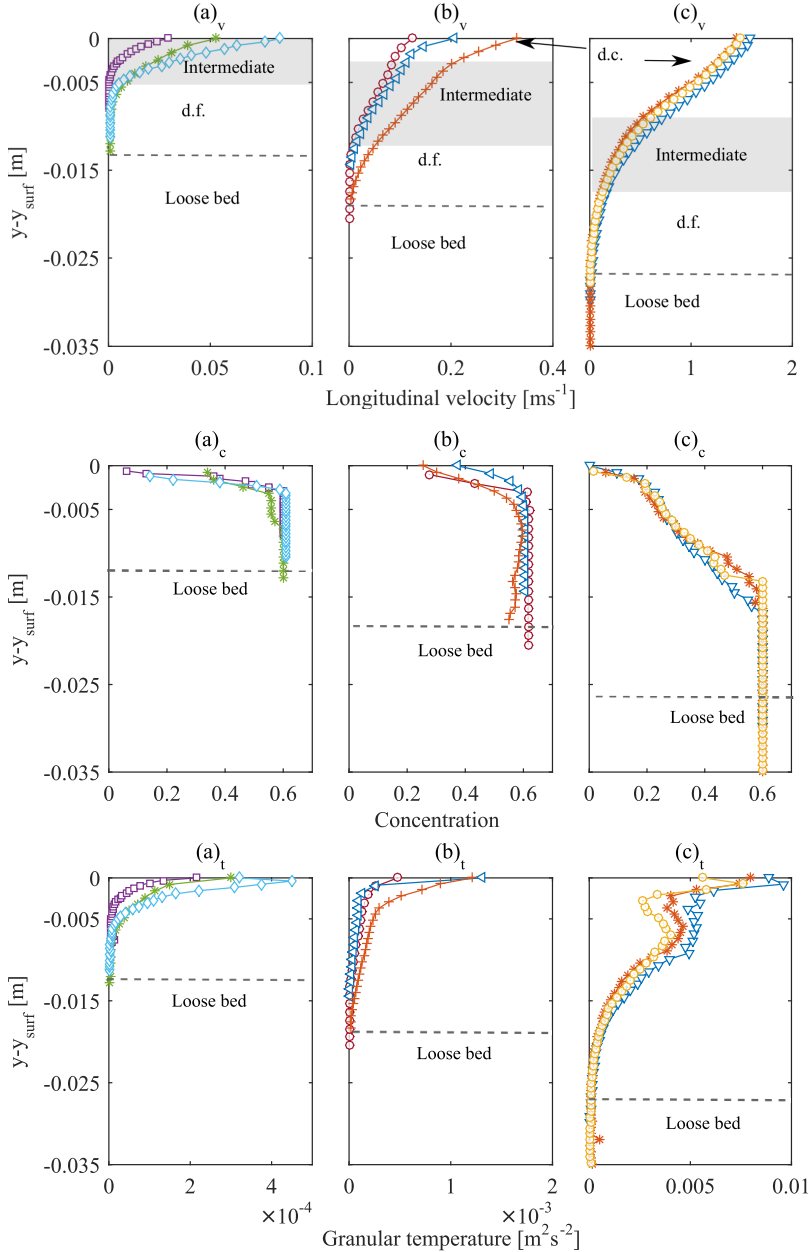


FIG. 3. Vertical profiles of velocity, concentration, and granular temperature for three different ranges of flow rate: (a) \square : $Q^* = 2.8, \alpha = 23.7^\circ$; $*$: $Q^* = 5.8, \alpha = 23.7^\circ$, \diamond : $Q^* = 6.8, \alpha = 23.8^\circ$; (b) \circ : $Q^* = 39.1, \alpha = 24.4^\circ$; \triangleleft : $Q^* = 46.2, \alpha = 24.9^\circ$; $+$: $Q^* = 82.4, \alpha = 25.87^\circ$; (c) \circ : $Q^* = 166.5, \alpha = 26.7^\circ$; $*$: $Q^* = 165.9, \alpha = 26.5^\circ$; ∇ : $Q^* = 182.9, \alpha = 27.8^\circ$. For each group, different types of grain interactions are highlighted along the vertical profiles: (i) flow dominated by collisions (d.c.), (ii) intermediate region, (iii) flow dominated by friction (d.f.), and (iv) loose bed.

calculating the level where the integral from the free surface of the product between concentration and velocity increases by less than 0.1%. The differences among the regimes are not very sharp, and they coexist in space and are intermittent in time [23].

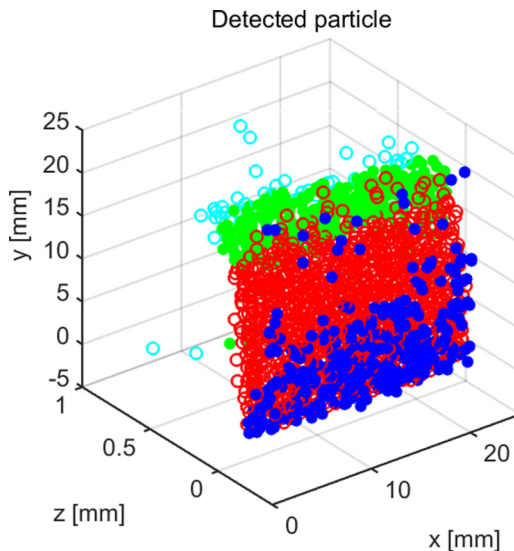


FIG. 4. Detected particles in a single frame using the three-dimensional Voronoi diagrams. The different colors are relative to particles with a different distance from the sidewalls: blue points: $0 < z_b < 0.03$ mm; red points: $0.03 < z_r < 0.2$ mm; green points: $0.2 < z_g < 0.4$ mm; and cyan points: $z_c > 0.4$ mm.

C. Free-surface profiles of velocity and granular temperature

Surface measurements are carried out adopting an optical filter to select all the grains contained in a volume having a depth of 1 particle diameter, above and below the focal plane. As already explained in Sec. III B, we identify the location of the free surface in the center of the layer within which the particle concentration falls below 0.01. This plane corresponds to the free surface, whose exact position is detected from the sidewalls.

As shown in Fig. 5(a), the velocity exhibits a symmetric profile across the width, reaching its maximum at the centerline and its minimum at the sidewalls. The trend is common for all the discharges that are analyzed and all the widths.

The free-surface granular temperature in Fig. 5(b) is computed considering the fluctuating components parallel to the motion and orthogonal to the sidewalls,

$$T = \frac{\langle u'^2 \rangle + 2\langle w'^2 \rangle}{3}, \quad (3)$$

where the z -direction fluctuating velocity component is assumed to be comparable in magnitude to the y -direction fluctuating velocity component, $\langle (w')^2 \rangle \simeq \langle (v')^2 \rangle$, as in [28] and as confirmed also by these experiments. It differs slightly from the granular temperature estimated from the lateral walls, where the three components are measured through stereoscopic recordings. As shown in Figs. 5(b) and 5(c), the granular temperature is almost constant across the width, except from the two bands near the lateral walls, where it increases. Here particles are subject to a double effect of the wall, which reflects the grain collisions and, at the same time, exerts a resistant action on the flow. As pointed out by [29], friction tends to reduce the mean velocity in the vicinity of the flat sidewalls, but its effect on the overall motion changes at different values of the vertical direction, following the variation of the velocity itself.

Therefore, near the surface where the flow is more dilute, the resistant action of the wall results in an increase of the granular temperature, as shown in Fig. 5(b), by increasing the particle rebounds. This, in turn, causes strong gradients of the longitudinal velocity as can be observed from the top of the flow, in the vicinity of the walls [Fig. 5(b)]. On the contrary, near the loose bed, the velocity

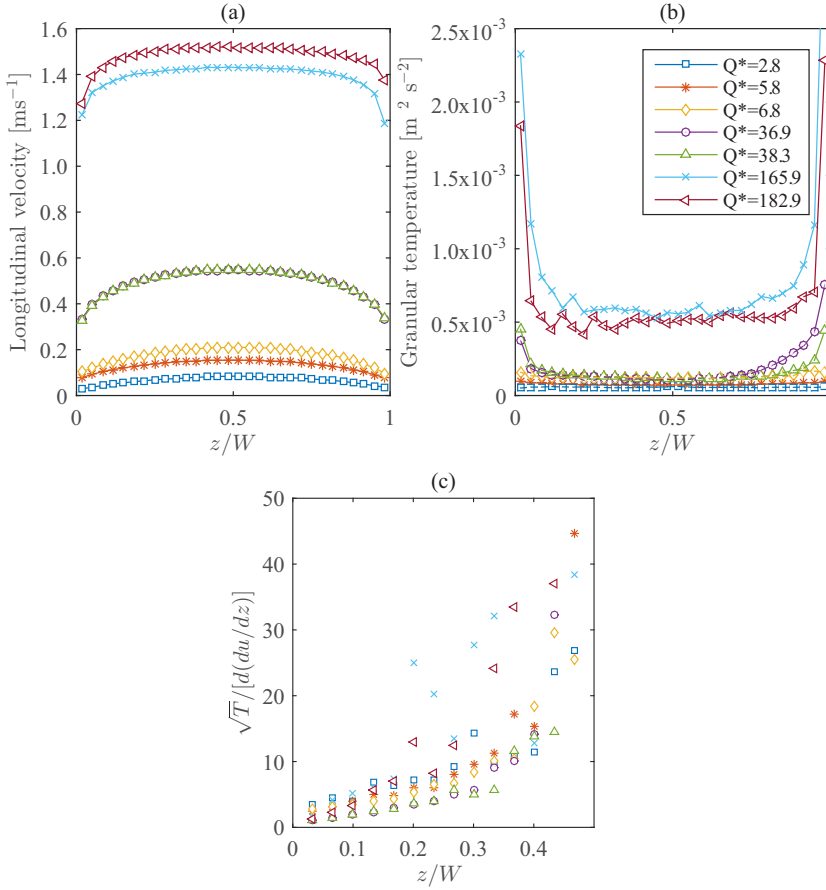


FIG. 5. Surface profiles for different flow rates: (a) longitudinal velocity and (b) granular temperature measured from the top of the flow; (c) granular temperature normalized with the “surface” shear rate $[d(du/dz)]$.

and energy production are low *per se*, and the lateral walls cause a further reduction of the velocity gradients and the temperature.

Figure 5(c) displays that the granular temperature at the free surface cannot be scaled with the free-surface shear rate at the sidewalls, as proven by the fact that the experimental points do not coalesce on the same curve. This is due to the diffusion of fluctuating energy from the shear zone, as also shown by [30] and [17] in their numerical simulations.

For very slow flows [see Fig. 5(b)], the temperature also remains almost constant near the walls due to the absence of the collisional layers.

The concentration profile is not reported since its quantitative estimation through the Voronoi method is not reliable from the two-dimensional analysis applied to the free surface since the technique has been calibrated in confined flows behind a transparent wall. The method only gives a qualitative profile of the particle distribution across the transversal direction.

D. Boundary conditions: Fixed and loose beds

The influence of the bed surface on the flow dynamics can be observed within the same experiment in which the first portion of the flow runs over a rigid bed, while the final part develops over a mobile bed made up of loose material, as sketched in Fig. 1. A first difference can be recognized in the macrofeatures of the uniform flows, which have the same slope of the flume when running over the

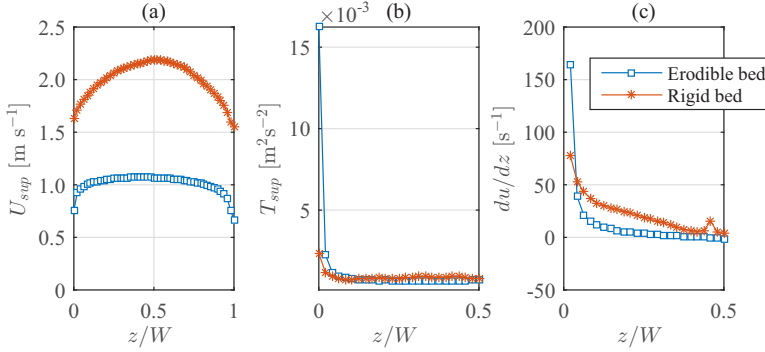


FIG. 6. Comparison of the transversal profiles between two base configurations: flow over an erodible bed and flow over a rigid and smooth bottom. (a) Longitudinal velocity from the top. (b) Granular temperature normalized with the mean longitudinal velocity. (c) Shear rate in the transverse direction. Both configurations refer to the same $Q^* = 185.38$. Note that in the section where the flow develops over a rigid bottom, the bed slope is that of the channel (i.e., 28°) and the free surface has nearly the same slope, while in the reach over the loose bed, the free-surface slope is milder (i.e., 25.2°) and the bed line is parallel to the free surface.

fixed bed, while it assumes the inclination of the deposit when developing over the mobile bed. In this case, the slope entirely depends on the discharge and on the flume width, being coupled on the flow dynamics. Therefore, increasing the flume inclination for the same discharge, in the fixed bed part the flow depth decreases and the velocity increases, while over the loose deposit they remain unchanged since only the volume of the deposit varies.

Going into detail, flows over a smooth, rigid bottom exhibit larger average velocities than over an erodible bed [Fig. 6(a)], which enhances the flow resistance since it absorbs and dissipates the fluctuation energy instead of reflecting it. In both cases, the surface longitudinal velocity is lower near the sidewalls than at the centerline, but in the presence of an erodible bed it is characterized by a more uniform central region, with an almost zero constant gradient [Fig. 6(c)]. In addition, as shown by the vertical profiles in Fig. 7(a), the presence of a loose deposit causes the longitudinal velocity to vanish towards the bed with an asymptotic tail, while a fix and smooth base produces a “Bagnold-type” profile, with a concave curvature and a nonzero slip velocity and gradient at the base [13,31]. For the conservation of mass, the flow that develops over an erodible bed is deeper than the flow over the smooth base, as clearly depicted by Fig. 7.

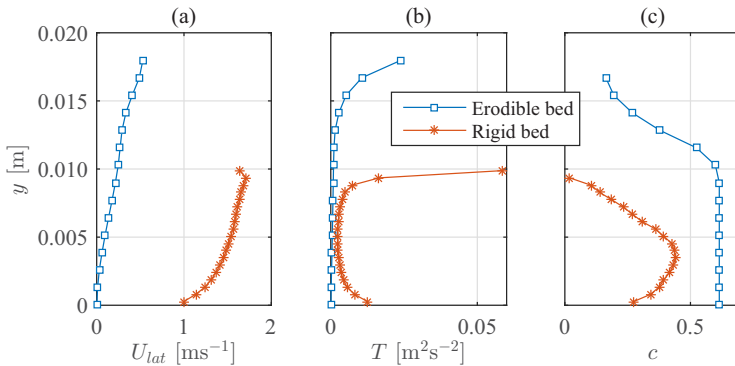


FIG. 7. Comparison of normal-to-bed profiles between two base configurations: flow over an erodible bed and flow over a rigid and smooth bottom from the lateral sidewalls. (a) Longitudinal velocity, (b) granular temperature, and (c) volume fraction profiles. Both configurations refer to the same $Q^* = 185.38$.

TABLE I. Investigated widths and corresponding dimensions in particle diameters.

W (cm)	W/d
1.5	25
2.0	33
2.5	42
3.0	50
3.5	58
5.0	83
15.0	250

The surface temperature exhibits the same trend for loose and rigid beds. However, the role of the bottom is clearly seen in the vertical profile of the temperature [Fig. 7(b)]. In fact, the granular temperature is nearly zero near the erodible bed, where grains are frozen in their static configuration, while it tends to increase near the rigid bed, where particles rebound against the solid base since the energy dissipation is lower and the streamwise velocity remains higher.

This trend is confirmed by the concentration profile measured at the sidewalls, which decreases near the smooth base as kinetic theory predicts [32] and some discrete element method (DEM) simulations showed [33,34], while it is almost constant at the lower layers in the other case.

However, even for flows over loose bed, it is reasonable to assume that the fluctuation energy and the solid volume fraction change from the lateral walls to the inside of the flow, taking their maxima at the center of the flume width, as observed by Hanes *et al.* [35] in their simulations on bumpy and rigid bases.

E. Effect of the sidewalls

A set of experiments was performed by changing the width of the channel in order to investigate the influence of the lateral confinement on the flow dynamics. Six different widths were analyzed and compared, as reported in Table I.

Observations are consistent with [6], which shows that the surface velocity increases by narrowing the channel at the same specific discharge, $Q^* = Q/dW\sqrt{gd}$. This means that when a flume is divided into two equal parts [see Fig. 8(a)], the resulting portions are characterized by larger values of the surface velocity (maximum and slip velocity at the sidewall) in comparison with the maximum speed measured in the undivided flume for the same Q^* . By contrast, the granular temperature in the central region of the flow [see Fig. 8(b)] seems to remain unchanged with the variation of the width. However, far from the sidewalls, a uniform part can always be observed, as represented in Figs. 9(a) and 9(b).

Figure 9(c) depicts the profiles of granular temperature on the free surface for two different widths. Near the walls there is a local increase of the temperature, and the extension of the region where this effect is relevant remains almost equal by changing the width under the same unit flow rate. The comparison of this boundary layer with the total width of the flume leads one to assume that the relative influence of the walls is higher for a narrower flume.

F. Free-surface slope

Figure 10 shows the variation of the free-surface slope at increasing values of the dimensionless discharge and for different channel widths.

The free-surface slope increases by narrowing the width, reaching a steady value for higher discharge. In our experiments, the maximum flow rate that could be obtained was limited by the volume of the hopper and by the extension of the channel, which was not long enough to allow for steady and uniform conditions in the case of very fast flows. Figure 10 also shows that for the same

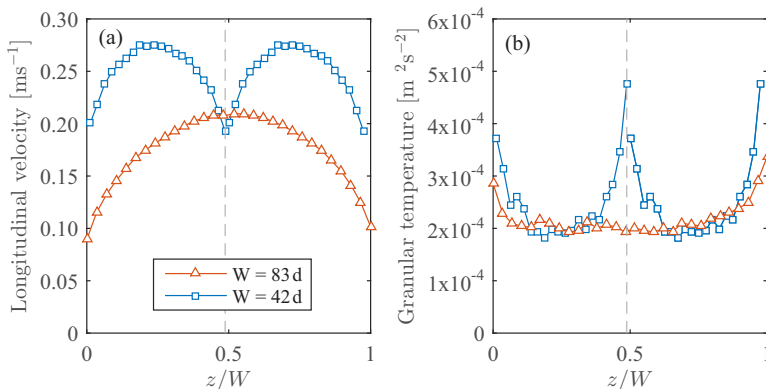


FIG. 8. Profiles of the longitudinal velocity and the granular temperature for two different widths ($W/d = 42$ and $W/d = 83$) and a single specific flow rate ($Q^* = 13.7$), depicted together as they were performed simultaneously in the flume. The gray line divides the channel into two equal parts of 2.5 cm each and represents the imagery sidewalls for the narrower channels. The z direction is normalized with respect to the channel width and spans from 0 to 1, while the granular temperature and the velocity are expressed in the international systems of units.

width, the free-surface slope increases with the discharge Q^* . This tendency has also been observed in [1,2,4,36,37] and its dependence on the width was first highlighted by the works of Refs. [5,6].

IV. DISCUSSION

Figure 11 reports the variation of the free-surface slope as a function of the ratio h/W . The colored symbols represent the experiments performed at the University of Trento, where the flow depth is measured at the wall, while the trends observed by [5] and [6] are depicted, respectively, by the dashed line and the solid line. A different trend can be highlighted between the experiments performed by Taberlet *et al.* [5] and the data obtained from our tests (in line with the findings of Jop *et al.* [6]). The disagreement might be due to the fact that the experiments in Ref. [5] were performed in narrow channels and at high flow rates. Therefore, with reference to Fig. 8(b), it is reasonable to assume that the central region of the granular flow, where the temperature is generally independent of the width, is almost zero in the case of the experiments of [5]. So the increase of the temperature due to the sidewall effect causes an increase of the energy production and of the free-surface slope.

A. Flow depth

In flows over a loose bed, although the free surface appears flat, the flow depth changes across the width, increasing towards the centerline where the surface velocity reaches its maximum. The variability of the flow field in the transverse direction can be estimated by the erosion method developed by Jop *et al.* [6]. In this regard, an example of the flow-depth profile estimated by the means of this technique is presented in Fig. 12(a) for a single width $W/d = 250$, but it can be considered significant for all the other widths. Albeit the method gives some insights into the flow-depth evolution across the width and on its correlation with the flow rate, its accuracy does not allow for a precise analysis of the flow far from the wall. In fact, a comparison between the flow depth measured through the erosion method and the height derived from the velocity profiles at the sidewall [Fig. 12(a)] shows that the erosion method might underestimate the depth where the particles are slower. Even if the flow depth observed from the transparent sidewall is not completely exhaustive because of the variability of this parameter along the transversal direction z , it is significant for the vertical evolution of the flow structure.

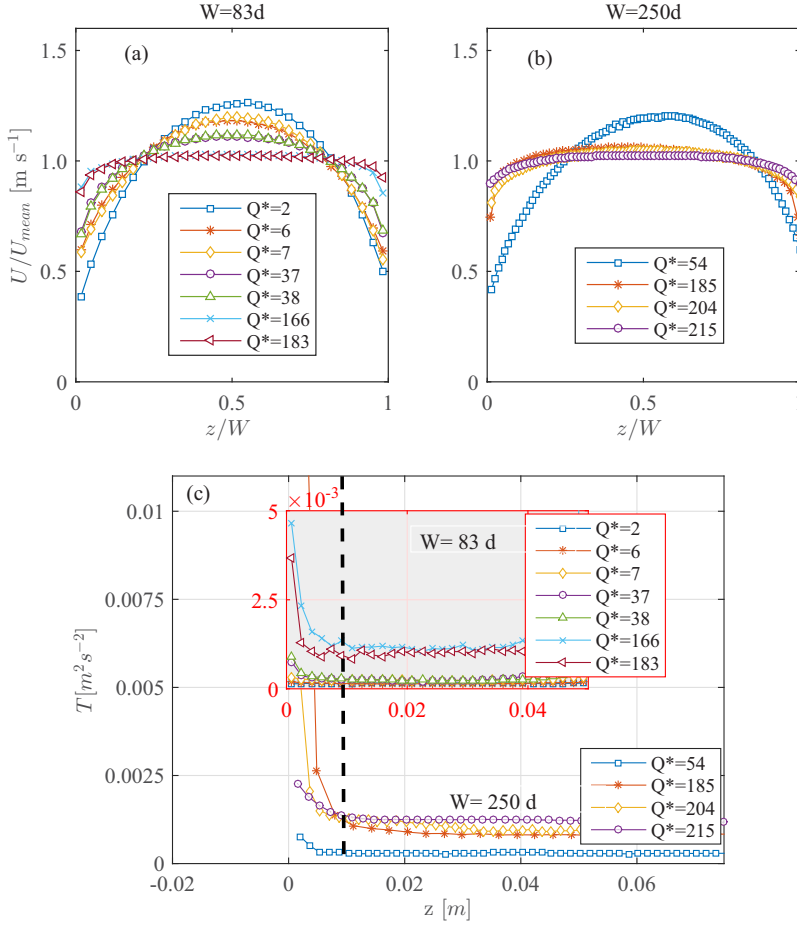


FIG. 9. Experiments for two different widths ($W = 83d$ and $W = 250d$). The plots represent (a),(b) the longitudinal velocity normalized with respect to the mean value and (c) the evolution of the granular temperature along the width. The dotted line in (c) represents the limit over which the effect of the sidewalls on the granular temperature starts to vanish.

Figure 12(b) shows the mean values of the flow depth measured through the erosion method for two separate widths, including the minimum value estimated close to the sidewalls and the maximum value measured at the centerline. Although the data are quite scattered, the deviation between the maximum depth and the minimum value was found to be larger for faster and wider flows (red circles), which are characterized by an increase of up to 45% of their depth going from the sidewalls to the center.

B. Hydraulic radius analogy

The definition of the flow depth adds complexity to the problem since it is not an independent parameter of the system, but is inherently coupled with the flow dynamics. In order to highlight the influence of the flow width on the flow depth, it is helpful to explore a possible analogy between the present granular flow and the steady uniform water flow in a rectangular channel. This analogy is not intended to be a new rheological model, but aims to better highlight the effect of the walls and the width on the resistance to flow by introducing the concept of hydraulic radius. This concept combines the resistance given by the erodible bed (soft and with a low bulk elasticity) with the

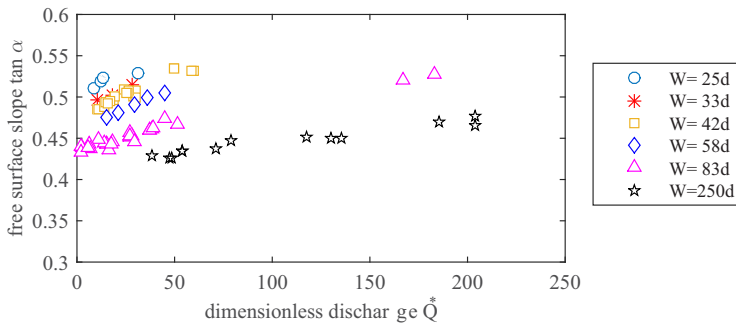


FIG. 10. Tangent of the angle measured between the free-surface slope and the horizontal as a function of the dimensionless discharge, $Q^* = Q/(W d \sqrt{dg})$. The different symbols refer to different widths, as indicated in the legend. All the data are collected in the flume developed at the University of Trento.

resistance given by the lateral sidewalls, which are more reflective and rigid. This point of view, which is commonly used in river hydraulics, emphasizes the relative importance of the sidewalls with respect to the erodible bed on the overall resistance to the flow motion.

For this purpose, we write the balance of the forces in the direction of the motion for a control volume that is laterally delimited by the sidewalls and below by the deposit, under the assumptions of steady and uniform condition:

$$\tau_f W + 2\tau_l \bar{h} = \rho_s g \Phi W \bar{h} \sin \alpha. \quad (4)$$

According to Eq. (4), the weight of the solid particles in the control volume is balanced by the friction at the bed τ_f over the deposit, and by the friction at the sidewalls τ_l , along the flow depth \bar{h} . In the expression, ρ_s is the density of the particles, W the width, Φ the solid concentration, and $\sin \alpha$ the free-surface slope, which is equal to the slope of the deposit for uniform conditions.

The shear stress might be defined in terms of the mean velocity of the flow depth, as is commonly done for water under uniform flow conditions. The generic friction stress can be written as

$$\tau_{(i)} \propto \rho_s f_{(i)} U^2, \quad (5)$$

where f is the friction factor that depends on the type of regime that characterizes the flow. The experimental observations suggest that particles move slowly near the deposit, where their motion

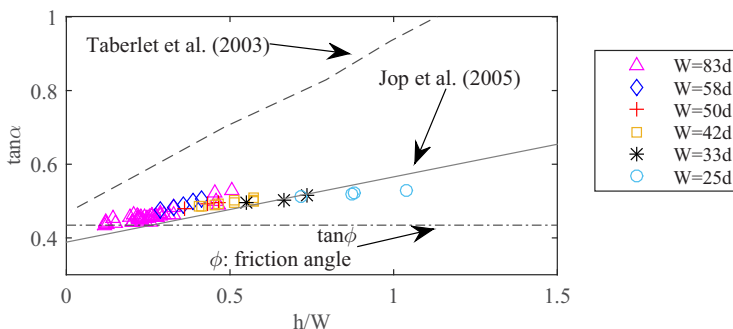


FIG. 11. Tangent of the free-surface slope against the ratio between the flow depth and width. Comparison of the experiments performed at the University of Trento (symbols) with the trend obtained by Jop *et al.* [6] (solid line) and Taberlet *et al.* [5] (dashed line). The friction angle of the plastic material used at the University of Trento is represented by the straight line $\tan \phi$.

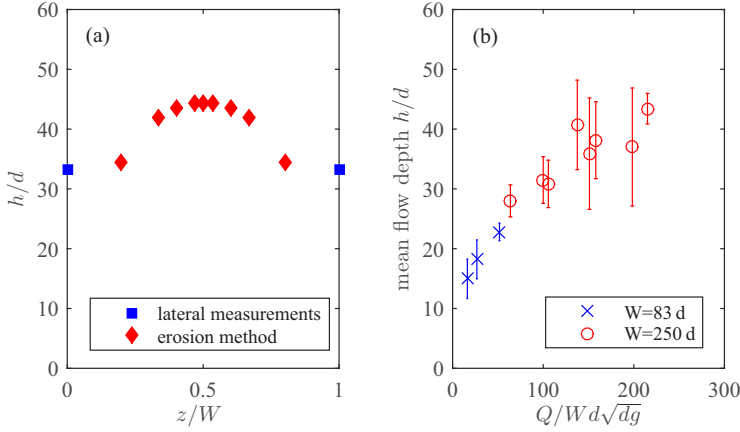


FIG. 12. (a) Profile of the flow depth across the width for $W = 250d$ obtained through the erosion method and from the lateral recordings. (b) Evolution of the flow depth with the flow rates for two different widths.

can be captured by a linear relation between velocity and shear stress, while they are more agitated near the sidewalls. Therefore, the following assumptions can be made for the coefficient $f_{(i)}$:

(1) At the interface between the flow and the static deposit, the regime can be similar to a viscous flow, so that the coefficient f_f may be defined in terms of the Reynolds number,

$$f_f \propto \frac{1}{Re} = \frac{\nu_g}{Ud}, \quad (6)$$

where ν_g is a suitable kinematic granular viscosity, with the same physical meaning of that of water.

(2) Near the sidewalls, the regime can be assumed to be similar to a turbulent flow on a rough wall, and f_l may be considered independent of the average velocity and it assumes a constant value, which can range between 0.001 and 1, as for water.

The relations for the friction stresses become

$$\tau_f \propto \rho_s \nu_g U/d, \quad \tau_l \propto \rho_s f_l U^2. \quad (7)$$

Substituting Eqs. (5)–(7) into Eq. (4), dividing all the term by (gdd) , and considering the following dimensionless variables:

$$U^* = \frac{U}{\sqrt{gd}}, \quad (8)$$

$$Q^* = \frac{Q}{Wd\sqrt{gd}} = U^* \frac{h}{d}, \quad (9)$$

$$W^* = W/d, \quad (10)$$

the force balance can be written as

$$U^* W^* \frac{1}{\frac{d\sqrt{gd}}{\nu_g}} + 2 f_l Q^* U^* = \Phi \frac{W^* Q^*}{U^*} \sin \alpha. \quad (11)$$

The free-surface slope can be expressed in terms of the ratio h/W , through a power relation whose coefficients can be fitted by the experimental data,

$$\sin \alpha = \sin \phi + a \left(\frac{h}{W} \right)^b, \quad (12)$$

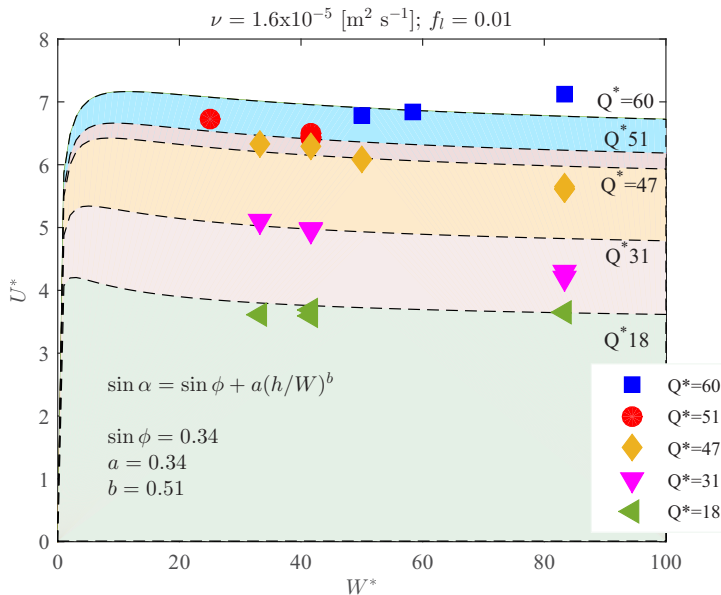


FIG. 13. Experimental points on the theoretical curves. All the parameters are reported on the plot.

with $b < 1$. Substituting in Eq. (11) and grouping the constant terms in the following coefficients:

$$A = \frac{v_g}{d\sqrt{gd}}, \quad B = 2f_l, \quad C = \Phi \sin \phi, \quad D = \Phi a, \quad (13)$$

the force balance becomes an expression of the dimensionless velocity in terms of the dimensionless width, through the parameter Q^* ,

$$U^*(AW^* + BQ^*) - \frac{CW^*Q^*}{U^*} + DW^{*(1-b)}Q^{*(1+b)}U^{*-(1+b)} = 0. \quad (14)$$

The above equation has been plotted in Fig. 13 using the constants listed in Table II. The friction factors v_g and f_l are obtained by calibrating their value in order to make the theoretical curves best fit the experimental data.

The simple expression shows that the velocity U^* always has a maximum in the transition between the *viscouslike* regime and the *turbulentlike* one. Additionally, it predicts the velocity reduction with the width and the tendency towards an asymptotic value for each discharge, independently of the width. The initial peak tends to be less sharp but higher as the viscosity decreases.

TABLE II. Parameters used in Eq. (14). The constants a and b have been fitted by the experimental data.

Symbol	Units	Value
d	m	0.00055
v_g	$\text{m}^2 \text{s}^{-1}$	1.6×10^{-5}
f_l		0.01
a		0.74
b		0.169
Φ		0.6

In Fig. 13, the experimental points have been superimposed on the curves computed according to Eq. (14) by choosing a proper value for the viscosity. Although expression (14) does not represent a model to predict the velocity since it was derived without a proper rheology, the comparison between the theoretical curves and the data is quite significant. The maximum of the velocity exhibited by the experimental points at lower values of the width is reproduced adequately by the expression.

The main differences arise at larger widths where the experimental data seem to increase faster than what is suggested by the expression. It might be due to the function chosen to define the free-surface slope, which is not appropriate to predict low ratios of the flow depth over the width.

V. CONCLUSIONS

The paper presents the results of a series of experiments involving dry granular material running on a loose bed driven by gravity and under steady and uniform conditions. The characteristic profiles of concentration, mean velocity, and granular temperature have been measured both through the sidewalls and from above the free surface. The experimental data have highlighted the following aspects:

(1) Uniform channel flow conditions can be obtained for a dry granular material, provided that the channel is adequately long and the boundary conditions are opportunely set to minimize the disturbance effects at the inlet and outlet sections of the channel.

(2) Flows over an immobile loose bed differ considerably from the flows over a rigid bed, where particles are in contact with the rigid bottom of the flume. In particular, in the latter case in a uniform condition, the free-surface slope is parallel to the channel inclination, while it depends on the flow rate and the lateral confinement if the flow develops over a loose material.

(3) The flow structures change with increasing flow rates. Passing from slow to fast runs, the flow evolves from a state dominated by prolonged interparticle contacts ($Q^* < 10$) to a state in which binary collisions occurring in the upper layers affect the entire flow depth ($Q^* > 150$).

When grain interactions become more collisional, the diffusion of the kinetic energy from the surface to the lower layers can be considered responsible for the strong gradients of the concentration. An intermediate state exists between these two ranges where particles alternate between long-lasting and instantaneous collisions.

(4) Lateral walls have a remarkable influence on the flow, especially for channels that are narrow compared with the grain size ($W/d < 10$). Surface measurements showed that the surface shear rates are present throughout the entire width for low values of flow rates ($Q^* < 10$), while they are located near the walls for high flow rates ($Q^* > 150$), being negligible in the central region of the width. In this respect, the behavior of dry granular flows is similar to a liquid flow in an open channel for different aspect ratio h/W . Additionally, under the same conditions of flow rate, narrower channels exhibit larger velocity, as also shown in Ref. [6], even if the measured granular temperature is comparable in the two different configurations. Considering the simple experience in which a channel is divided into two equal parts and in analogy to the water, the increase of the surface velocity for the same flow rate implies that the shear stress at the immobile bed plays a major role with respect to the stress at the lateral walls. In particular, doubling the walls in the computation of the hydraulic radius does not have a proportional effect on the global resistance to the flow, at least in the range of the analyzed widths ($W/d = 42 \div 250$). The effect of the confinement produces an increase of the free-surface slope for decreasing values of the width, as also seen in Ref. [5].

(5) The analogy with the river hydraulics shows that the lateral walls influence the mechanisms of friction and energy dissipation as long as the ratio W/d remains adequately low, presumably because of the formation of particle chains between the walls or because of the effect of particle rebound exert by the lateral walls [Fig. 8(b)], in conjunction with larger aspect ratios h/W within the flow.

An aspect that is worth analyzing experimentally in the future is the role of the wall roughness in the lateral confinement, and what happens if this is equal to the roughness of the loose bed. Such configuration could be more similar to what occurs in nature, where the lateral confinements are made up of the same material composing the flow. An additional effort should be paid to quantify

the stresses at the walls and the base in order to establish the relative weight to the global resistance to the flow.

ACKNOWLEDGMENT

S.M. has been funded by DICAM-CUDAM, Università di Trento, Contract Grant No. 30103490.

-
- [1] J. Rajchenbach, Flow in Powders: From Discrete Avalanches to Continuous Regime, *Phys. Rev. Lett.* **65**, 2221 (1990).
 - [2] P. A. Lemieux and D. J. Durian, From Avalanches to Fluid Flow: A Continuous Picture of Grain Dynamics Down a Heap, *Phys. Rev. Lett.* **85**, 4273 (2000).
 - [3] C. Ancey and P. Evesque, Frictional-collisional regime for granular suspension flows down an inclined channel, *Phys. Rev. E* **62**, 8349 (2000).
 - [4] D. V. Khakhar, A. V. Orpe, P. Andresén, and J. M. Ottino, Surface flow of granular materials: Model and experiments in heap formation, *J. Fluid Mech.* **441**, 255 (2001).
 - [5] N. Taberlet, P. Richard, A. Valance, W. Losert, J. M. Pasini, J. T. Jenkins, and R. Delannay, Superstable Granular Heap in a thin Hannel, *Phys. Rev. Lett.* **91**, 264301 (2003).
 - [6] P. Jop, Y. Forterre, O. Pouliquen *et al.*, Crucial role of sidewalls in granular surface flows: Consequences for the rheology, *J. Fluid Mech.* **541**, 167 (2005).
 - [7] W. Bi, R. Delannay, P. Richard, N. Taberlet, and A. Valance, Two- and three-dimensional confined granular chute flows: Experimental and numerical results, *J. Phys.: Condens. Matter* **17**, S2457 (2005).
 - [8] N. Mitarai and H. Nakanishi, Bagnold Scaling, Density Plateau, and Kinetic Theory Analysis of Dense Granular Flow, *Phys. Rev. Lett.* **94**, 128001 (2005).
 - [9] L. E. Silbert, D. Ertas, G. S. Grest, T. C. Halsey, D. Levine, and S. J. Plimpton, Granular flow down an inclined plane: Bagnold scaling and rheology, *Phys. Rev. E* **64**, 051302 (2001).
 - [10] T. S. Komatsu, S. Inagaki, N. Nakagawa, and S. Nasuno, Creep Motion in a Granular Pile Exhibiting Steady Surface Flow, *Phys. Rev. Lett.* **86**, 1757 (2001).
 - [11] GDR-MiDi, On dense granular flows, *Eur. Phys. J. E* **14**, 341 (2004).
 - [12] R. Delannay, M. Louge, P. Richard, N. Taberlet, and A. Valance, Towards a theoretical picture of dense granular flows down inclines, *Nat. Mater.* **6**, 99 (2007).
 - [13] O. Pouliquen, Scaling laws in granular flows down rough inclined planes, *Phys. Fluids* **11**, 542 (1999).
 - [14] G. Koval, J.-N. Roux, A. Corfdir, and F. Chevoir, Annular shear of cohesionless granular materials: From the inertial to quasistatic regime, *Phys. Rev. E* **79**, 021306 (2009).
 - [15] V. Kumaran and S. Bharathraj, The effect of base roughness on the development of a dense granular flow down an inclined plane, *Phys. Fluids* **25**, 070604 (2013).
 - [16] L. E. Silbert, J. W. Landry, and G. S. Grest, Granular flow down a rough inclined plane: transition between thin and thick piles, *Phys. Fluids* **15**, 1 (2003).
 - [17] R. Artoni and P. Richard, Effective Wall Friction in Wall-Bounded 3d Dense Granular Flows, *Phys. Rev. Lett.* **115**, 158001 (2015).
 - [18] J. T. Jenkins and S. B. Savage, A theory for the rapid flow of identical, smooth, nearly elastic, spherical particles, *J. Fluid Mech.* **130**, 187 (1983).
 - [19] J. T. Jenkins, Boundary conditions for rapid granular flow: Flat, frictional walls, *J. Appl. Mech.* **59**, 120 (1992).
 - [20] M. W. Richman, Boundary conditions based upon a modified Maxwellian velocity distribution for flows of identical, smooth, nearly elastic spheres, *Acta Mech.* **75**, 227 (1988).
 - [21] G. Lois, A. Lemaitre, and J. M. Carlson, Emergence of multi-contact interactions in contact dynamics simulations of granular shear flows, *Europhys. Lett.* **76**, 318 (2006).
 - [22] A. Armanini, H. Capart, L. Fraccarollo, and M. Larcher, Rheological stratification in experimental free-surface flows of granular-liquid mixtures, *J. Fluid Mech.* **532**, 269 (2005).

- [23] A. Armanini, M. Larcher, and L. Fraccarollo, Intermittency of rheological regimes in uniform liquid-granular flows, *Phys. Rev. E* **79**, 051306 (2009).
- [24] H. Capart, D. L. Young, and Y. Zech, Voronoi imaging methods for the measurement of granular flows, *Exp. Fluids* **32**, 121 (2002).
- [25] B. Spinewine, H. Capart, M. Larcher, and Y. Zech, Three-dimensional Voronoi imaging methods for the measurement of near-wall particulate flows, *Exp. Fluids* **34**, 227 (2003).
- [26] K. M. Hill, G. Gioia, and V. V. Tota, Structure and Kinematics in Dense Free-Surface Granular Flow, *Phys. Rev. Lett.* **91**, 064302 (2003).
- [27] S. Meninno, Mechanics of dry granular flows driven by gravity, Ph.D. thesis, University of Trento, 2015.
- [28] N. Jesuthasan, B. R. Baliga, and S. B. Savage, Use of particle tracking velocimetry for measurements of granular flows: Review and application, *KONA Powder Part. J.* **24**, 15 (2006).
- [29] H. Xu, M. Louge, and A. Reeves, Solutions of the kinetic theory for bounded collisional granular flows, *Continuum Mech. Thermodyn.* **15**, 321 (2003).
- [30] R. Artoni, A. Santomaso, and P. Canu, Effective boundary conditions for dense granular flows, *Phys. Rev. E* **79**, 031304 (2009).
- [31] E. Azanza, F. Chevoir, and P. Moucheron, Experimental study of collisional granular flows down an inclined plane, *J. Fluid Mech.* **400**, 199 (1999).
- [32] M. Y. Louge and S. C. Keast, On dense granular flows down flat frictional inclines, *Phys. Fluids* **13**, 1213 (2001).
- [33] T. Börzsönyi, R. E. Ecke, and J. N. McElwaine, Patterns in Flowing Sand: Understanding the Physics of Granular Flow, *Phys. Rev. Lett.* **103**, 178302 (2009).
- [34] N. Brodu, P. Richard, and R. Delannay, Shallow granular flows down flat frictional channels: Steady flows and longitudinal vortices, *Phys. Rev. E* **87**, 022202 (2013).
- [35] D. M. Hanes and O. R. Walton, Simulations and physical measurements of glass spheres flowing down a bumpy incline, *Powder Technol.* **109**, 133 (2000).
- [36] C. M. Dury, G. H. Ristow, J. L. Moss, and M. Nakagawa, Boundary effects on the angle of repose in rotating cylinders, *Phys. Rev. E* **57**, 4491 (1998).
- [37] Y. Grasselli and H. J. Herrmann, Shapes of heaps and in silos, *Eur. Phys. J. B* **10**, 673 (1999).